International Journal on Magnetic Particle Imaging
Vol 9, No 1, Suppl 1, Article ID 2303077, 4 Pages

Infinite Science Publishing

Proceedings Article

Deconvolution of direct reconstructions for MPI using Convolutional Neural Network

Mathias Eulers[a,*] · Christine Droigk[a] · Marco Maass[a] · Alfred Mertins[a,b]

[a]Institute for Signal Processing, Universität zu Lübeck, Lübeck, Germany
[b]German Research Center for Artificial Intelligence (DFKI), AI in Biomedical Signal Processing, Lübeck, Germany
*Corresponding author, email: m.eulers@uni-luebeck.de

Abstract

Recently, an approach was presented that allows a direct and fast image reconstruction without the use of a system matrix for Lissajous trajectories of the so called field free point. The method is based on weighting frequency components of the measured voltage signals and additional factors with Chebychev polynomials of the second kind, resulting in reconstructions of the convolved spatial distribution of magnetic nanoparticles. In order to obtain meaningful images, these reconstructions have to be deconvolved afterwards. For this purpose, different methods have already been proposed. In this work, a U-shaped neural network is used for the deconvolution. The network was trained and tested on simulated data of blood vessel like structures. The proposed model outperforms conventional methods and improves the image quality of the reconstructions.

I. Introduction

Magnetic particle imaging (MPI) is a non-invasive tomographic medical imaging modality. Superparamagnetic nanoparticle tracers (SPIO) are directly detected within biological fluids, such as blood, by measuring the voltage induced through the magnetization changes of the magnetic nanoparticle distribution [1]. Often, a measured system function describing the relationship between the received signal and the nanoparticle distribution is used for image reconstruction.
A recently presented method in [2] proposed a fast direct reconstruction of two- and three-dimensional SPIO distributions. The method weights frequency components of the voltage signals with Chebyshev polynomials of second kind, followed by a deconvolution step. Except for the estimation of the transfer function, the method does not need a system matrix, but has drawbacks regarding the image quality, as the deconvolution step could introduce noise-dependent image artifacts in the reconstruction results.
For this reason, in this work a neural network model based on a U-Net architecture is proposed to perform the deconvolution step. The presented network is evaluated on a data set consisting of images of simulated blood vessel like structures and compared with the conventional deconvolution methods from [2].

II. Methods and materials

The direct Chebychev polynomial based reconstruction method proposed in [2] is derived from the two- and three-dimensional system function in Fourier space for the Langevin model of paramagnetism with Lissajous-type excitation patterns. Due to space constraints, we will only briefly introduce the method for the two-dimensional case with an x- and y-coil in this work and refer to [2] for a more detailed description.
The two-dimensional case can be shortly described in few steps. First, the frequency components $\hat{u}_{ik}$ of Fourier transformed voltage signals with $i \in 1,2$ of two receiv-

10.18416/ijmpi.2023.2303077

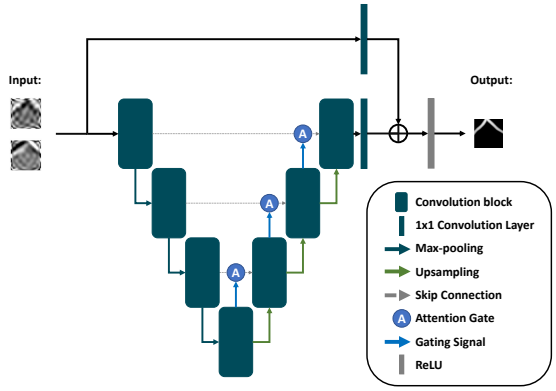

Figure 1: Block diagram of the proposed U-Net model.

ing coils are mapped to the orders of Chebyshev polynomials. Subsequently, as indicated in [2, Eq.(25)], the reconstruction approximates the convolved particle distribution $\tilde{c}_i(\mathbf{x})$ by summation of tensor products of Chebyshev polynomials of second kind weighted with the corresponding frequency components of $\hat{u}_{ik}$ for each coil. Because the approximated particle distributions equal the true distributions convolved with the derivative of the Langevin function [3], both reconstructions $\tilde{c}_i(\mathbf{x})$ have to be rescaled, deconvolved and combined to a single image afterwards. The rescaling can be done according to [2, Eq. (19)].

For the deconvolution and fusion of $\tilde{c}_i(\mathbf{x})$ two methods were proposed in [2], one kernel-based technique, referred as to the SLE deconvolution, and another one, which uses no explicit kernel, referred to as cumsum deconvolution. Since the SLE deconvolution treats the decovolution task as a minimization problem, see [2, Eq. (39)], which can be solved analytically or iteratively, this method is further distinguished into SLE-ℓ_1 for the iterative solution with an ℓ_1-regularization and SLE-ℓ_2 for the analytical solution with an ℓ_2-regularization of the minimization problem.

II.I. Convolutional Neural Network

In this work, we propose a neural network model to perform the deconvolution. The proposed model is derived from the U-Net model in [4]. The inputs of the network are the normalized real parts of $\tilde{c}_i(\mathbf{x})$ as input channels, resulting in an input of shape $H \times W \times 2$. The original model is based on the typical structure of U-Nets enhanced by attention gates. In the encoding part the input is subsequently processed by convolution blocks consisting of two convolution layers followed by a batchnorm and a ReLU acitvation function each. In the first layer of every block the number of feature maps is increased from 64 after the first one to 512 overall, while the spatial dimensions are downsampled by a factor 2 using max-pooling after every block.

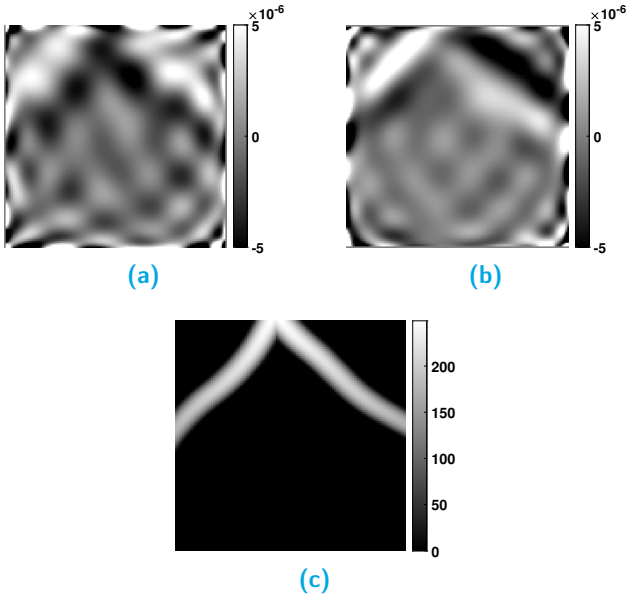

Figure 2: Example of $\tilde{c}_1$ for the x-coil (a) and $\tilde{c}_2$ for the y-coil (b). For better visibility of the structures, the value range of the pixels was constrained to $-5 \cdot 10^{-6}$ to $5 \cdot 10^{-6}$. In (c), the corresponding ground truth image is shown.

In the decoder part the spatial dimensions are restored and the number of feature maps is reduced to one. In this work, we extended the model from [4] by a shortcut connection with a convolution Layer with kernel size 1×1 and an additional ReLu at the end. The input is passed through the shortcut connection to fuse $\tilde{c}_i(\mathbf{x})$ to a single channel feature map and therefore enable the network to learn a fitting residual mapping to predict the deconvolved distribution $c(x)$. An overview of the network is depicted in Fig. 1.

III. Experiments

The proposed neural network was trained and tested using an MPI-scanner simulation to generate training and test data. The simulation follows the Langevin model of paramagnetism, excluding relaxation effects. A Lissajous-type excitation pattern with frequency ratio $f_x/f_y = 33/32$ was used, the particle size was set to 30 nm and temperature to 293 K. In this way 7000 simulated voltage signals were created. To obtain more realistic signals, these were corrupted by signal-independent Gaussian noise, resulting in a signal-to-noise ratio (SNR) between 15 dB and 40 dB. However, as in [2], a thresholding with a threshold $\tau = 250$ was applied for each frequency component k to exclude frequency components with poor SNR. Using the direct reconstruction algorithm from Sec. II, 7000 convolved SPIO distributions for the x- and y-coils were reconstructed from the

10.18416/ijmpi.2023.2303077

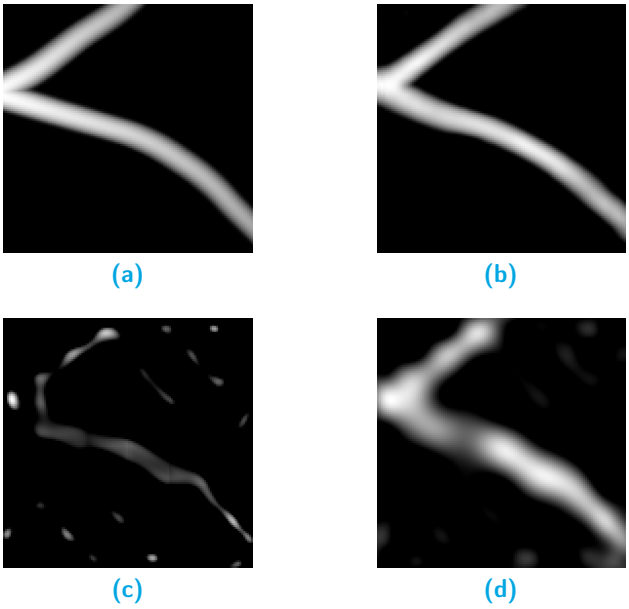

Figure 3: An example ground truth image of the test data set (a). The prediction of the U-Net model (b) and the solution of the SLE-ℓ_1 (c) and SLE-ℓ_2 (d) deconvolution.

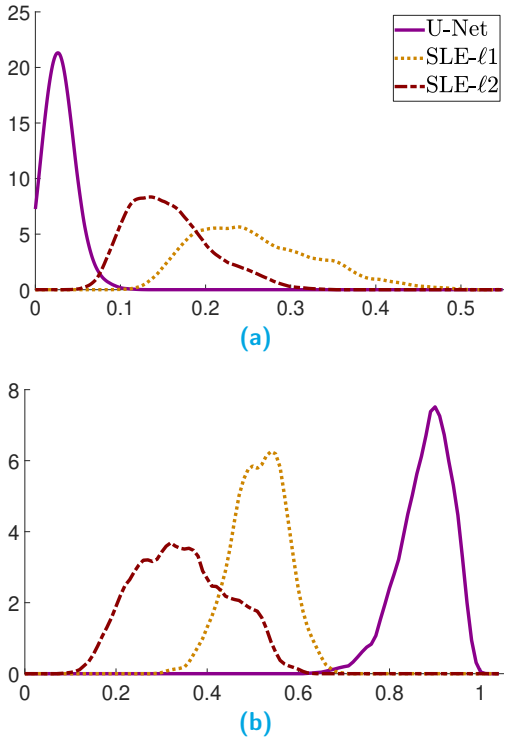

Figure 4: Estimated probability density function of the predictions of the U-Net, SLE-ℓ_1 and SLE-ℓ_2 deconvolution regarding MSE (a) and SSIM (b).

Table 1: Quantitative results of the U-Net model, SLE-ℓ_1 and SLE-ℓ_2 deconvolution.

		U-Net	SLE-ℓ_1	SLE-ℓ_2
MSE	Mean	0.029	0.259	0.158
	Median	0.027	0.247	0.151
	SD	0.015	0.072	0.048
SSIM	Mean	0.88	0.51	0.35
	Median	0.88	0.52	0.34
	SD	0.056	0.060	0.101

simulated voltage signals.
So, in total, the data set consists of 7000×2 convolved images containing blood vessel like structures with a size 128×128 pixels. 5000 images were used for the training of the neural network, 700 for validation and 1300 for testing of the model. An example from the training dataset is shown in Fig. 2. The model was trained using the Adam optimizer with the mean absolute error (MAE) as objective function and a learning rate of 10^{-4}, which was decayed by 0.9 after every 30-th epoch. The training process was stopped when no improvement was observed, so the training lasted 345 epochs. In every epoch all training data were randomly divided into batches containing 20 training samples. To reduce the risk of overfitting the training data were randomly rotated by 90°, 180° or 270° degrees in every epoch.

IV. Results and discussion

The trained neural network was compared to the two SLE deconvolution methods and the cumsum deconvolution from [2, Sec. 2.3]. Since the results of the SLE deconvolution are highly dependent on the choice of an appropriate regularization parameter λ, see [2, Eq. (39)], we chose λ in both cases to minimize the average error on the test data. Therefore, values in the range from 10^{-5} to 10^5 for SLE-ℓ_1 and values in the range from 10^5 to 10^{15} for SLE-ℓ_2 in steps of 10^1 were tested. A minimal average MAE was achieved with $\lambda = 10^3$ for SLE-ℓ_1 and $\lambda = 10^{10}$ for SLE-ℓ_2. For SLE-ℓ_1 the minimization problem was solved by the fast iterative shrinkage thresholding algorithm (FISTA) [5]. Moreover, it became evident that, due to the noise no suitable parameters could be found for the cumsum method to obtain reasonable results. The results were significantly worse than for the other methods, as it was already the case in [2]. Therefore, a detailed presentation of these results will be omitted here. To compare the deconvolution methods, two error measures, the mean squared error (MSE) and the structural similarity index (SSIM)[6] were calculated. For both metrics, the median, average and standard deviation (SD) over the whole test data set is shown in Table 1. The U-Net model outperforms both SLE deconvolution methods. The results show an improvement in both metrics, which is also

reflected in an improvement in the visual image quality. An example prediction for all methods is depicted in Fig. 3. Furthermore, in order to better visualize differences in performance between the methods, probability density functions (PDF) based on a kernel density estimation regarding the MSE and SSIM of all predictions of the three methods were computed using an Epanechinkov kernel with a bandwidth of 0.012. The PDFs are shown in Fig. 4. The PDFs support an assumption which is also indicated by the calculated standard deviations, specifically the lowest variance can be expected for the predictions of the U-Net. Furthermore, it can be assumed that in almost all cases the predictions of the U-Net will have a lower MSE or a higher SSIM than the predictions of the other methods.

V. Conclusion

The experiments performed on simulated data in this work show a possible way to enable fast and high-quality image reconstructions in MPI. Therefore, in the recently proposed method for direct image reconstruction in [2] the conventional deconvolution methods were replaced with a dedicated U-Net model. The presented U-Net was able to outperform the conventional methods on simulated data of blood vessel like structures.
The U-Net achieved the highest image quality of all methods on the test data. However, in order to better evaluate the general applicability of the presented approach, experiments on real-world data and with different parameter setting in the reconstruction process should be performed. Furthermore, it can be expected that the network architecture could be further optimized to achieve more stable deconvolution results.

Author's statement

Authors state no conflict of interest.

References

[1] B. Gleich and J. Weizenecker. Tomographic imaging using the nonlinear response of magnetic particles. *Nature*, 435(7046):1214–1217, 2005, doi:10.1038/nature03808.

[2] C. Droigk, M. Maass, and A. Mertins. Direct multi-dimensional Chebyshev polynomial based reconstruction for magnetic particle imaging. *Physics in Medicine & Biology*, 67(4):045014, 2022, doi:10.1088/1361-6560/ac4c2e.

[3] M. Maass and A. Mertins. On the representation of magnetic particle imaging in Fourier space. *International Journal on Magnetic Particle Imaging*, 6(1), 2020.

[4] O. Oktay, J. Schlemper, L. L. Folgoc, M. Lee, M. Heinrich, K. Misawa, K. Mori, S. McDonagh, N. Y. Hammerla, B. Kainz, B. Glocker, and D. Rueckert, Attention U-Net: Learning where to look for the pancreas, in *Medical Imaging with Deep Learning*, 2018. doi:10.48550/ARXIV.1804.03999.

[5] A. Beck and M. Teboulle. A fast iterative shrinkage-thresholding algorithm for linear inverse problems. *SIAM Journal on Imaging Sciences*, 2(1):183–202, 2009, doi:10.1137/080716542.

[6] Z. Wang, A. Bovik, H. Sheikh, and E. Simoncelli. Image quality assessment: From error visibility to structural similarity. *IEEE Transactions on Image Processing*, 13(4):600–612, 2004, doi:10.1109/TIP.2003.819861.

